

# 1 Contrast sensitivity with a subretinal prosthesis and implications 2 for efficient delivery of visual information

3 Georges Goetz<sup>1,2</sup>, Richard Smith<sup>4</sup>, Xin Lei<sup>2</sup>, Ludwig Galambos<sup>2</sup>, Theodore Kamins<sup>2</sup>,  
4 Keith Mathieson<sup>5</sup>, Alexander Sher<sup>† 4</sup>, Daniel Palanker<sup>† 1,3</sup>

5  
6 <sup>1</sup>Hansen Experimental Physics Laboratory, <sup>2</sup>Department of Electrical Engineering,,<sup>3</sup>Department of  
7 Ophthalmology Stanford, CA 94305, USA.

8 <sup>4</sup>Santa Cruz Institute for Particle Physics, University of California Santa Cruz, Santa Cruz, CA 95064,  
9 USA.

10 <sup>5</sup>Institute of Photonics, University of Strathclyde, Glasgow, Scotland G4 0NW, UK.

11 **Word count:** Abstract 316 words, text 4556 words.

12 **Purpose:** To evaluate the contrast sensitivity of a degenerate retina stimulated by a photovoltaic  
13 subretinal prosthesis, and assess the impact of low contrast sensitivity on transmission of visual  
14 information.

15 **Methods:** We measure *ex-vivo* the full-field contrast sensitivity of healthy rat retina stimulated with  
16 white light, and the contrast sensitivity of degenerate rat retina stimulated with a subretinal  
17 prosthesis at frequencies exceeding flicker fusion (>20Hz). Effects of eye movements on retinal  
18 ganglion cell (RGC) activity are simulated using a linear-nonlinear model of the retina.

19 **Results:** RGCs adapt to high frequency stimulation of constant intensity, and respond transiently to  
20 changes in illumination of the implant, exhibiting responses to ON-sets, OFF-sets, and both ON- and  
21 OFF-sets of light. The percentage of cells with an OFF response decreases with progression of the  
22 degeneration, indicating that OFF responses are likely mediated by photoreceptors. Prosthetic vision  
23 exhibits reduced contrast sensitivity and dynamic range, with 65% contrast changes required to  
24 elicit responses, as compared to the 3% (OFF) to 7% (ON) changes with visible light. The maximum  
25 number of action potentials elicited with prosthetic stimulation is at most half of its natural  
26 counterpart for the ON pathway. Our model predicts that for most visual scenes, contrast sensitivity  
27 of prosthetic vision is insufficient for triggering RGC activity by fixational eye movements.

28 **Conclusions:** Contrast sensitivity of prosthetic vision is 10 times lower than normal, and dynamic  
29 range is two times below natural. Low contrast sensitivity and lack of OFF responses hamper  
30 delivery of visual information via a subretinal prosthesis.

31 **Financial disclosure:** D.P.'s patents related to retinal prostheses are owned by Stanford University  
32 and licensed to Pixium Vision. D.P. is a consultant for Pixium Vision.

33 **Funding sources:** Funding was provided by the National Institutes of Health (grant R01-EY-018608,  
34 D.P.), the Department of Defense (grant W81XWH-15-1-0009, D.P.) and the Stanford Spectrum fund  
35 (D.P). A.S. was supported by BWF CASI and Pew Charitable Trusts Scholarship in the Biomedical  
36 Sciences. K.M. was supported by an SU2P fellowship as part of an RCUK Science Bridges award.

# 1 Introduction

2 Retinal degenerative diseases such as age-related macular degeneration and retinitis pigmentosa are  
3 among the most common causes of untreatable blindness in the developed world<sup>1</sup>. In these diseases,  
4 the image-capturing photoreceptors degrade, while cells in the image-processing layers of the retina  
5 can remain relatively intact<sup>2-4</sup>, albeit with sometimes extensive rewiring<sup>5</sup>, allowing for the possibility  
6 of sight restoration via electrical stimulation of these surviving neurons. The epiretinal approach to  
7 retinal prostheses involves direct stimulation of the retinal ganglion cells (RGCs)<sup>6</sup>, while the  
8 subretinal approach primarily targets the bipolar cell layer<sup>7</sup>. With both approaches, prosthetic  
9 systems currently approved for clinical use involve cumbersome implants wired to extraocular  
10 power supplies, necessitating complex surgeries.

11 To address this issue, we developed a modular, easy-to-implant photovoltaic subretinal prosthesis  
12 system in which power and visual information are delivered directly to each pixel by light projected  
13 from video goggles<sup>7-9</sup>. The light is pulsed to provide bi-phasic charge-balanced stimulation<sup>10</sup> required  
14 for electrochemical biocompatibility. Use of a near-infrared wavelength (880-915nm) allows  
15 avoiding both photophobic and phototoxic effects of bright illumination. Processing of the visual  
16 signal between the camera and the head-mounted display can be individually tailored to each  
17 patient.

18 A recent study has demonstrated both *ex-* and *in-vivo* that the resolution of this implant corresponds  
19 to its 65 $\mu$ m pixel pitch<sup>11</sup>. However, it did not address the problem of delivering multiple gray levels  
20 to the implant. In the present paper, we therefore consider retinal responses to changes in luminance  
21 over the array, comparing the full-field contrast sensitivity of prosthetic stimulation of degenerate  
22 rat retina with that of normal vision in healthy retinas. Since the contrast sensitivity with subretinal  
23 electrical stimulation was found to be much lower than normal, we explore through simulations the  
24 implications of this finding for efficient delivery of visual information.

25 In the case of normal vision, the statistics of natural scenes, fixational eye movements (FEMs) and the  
26 contrast sensitivity of retinal ganglion cells are all well-tuned to each other and enable efficient

1 encoding of the visual signal<sup>12, 13</sup>. We show that the reduced contrast sensitivity and lack of OFF  
2 responses in prosthetic vision introduces a mismatch in this encoding machinery. We predict that the  
3 majority of FEMs cannot trigger RGC responses with such low contrast sensitivity, which could  
4 explain image fading at high stimulation frequencies in patients with subretinal prostheses<sup>14</sup>.

## 5 **Methods**

### 6 ***Implant fabrication***

7 We manufactured photovoltaic arrays on silicon-on-insulator wafers using a six-mask lithographic  
8 process, as described previously<sup>15</sup>. To produce anodic-first pulses of electric current, we reversed the  
9 n-doped and p-doped regions in the diodes compared to the previous description. Photovoltaic  
10 arrays consisted of 70 or 140  $\mu\text{m}$  pixels, separated by 5 $\mu\text{m}$  trenches. Each pixel contained two  
11 photodiodes connected in series between the active and return electrodes arranged in a hexagonal  
12 array. A resistance between the active and return electrodes helps discharge them between the light  
13 pulses, thus achieving charge balance.

### 14 ***Electrophysiological recordings***

15 We obtained rats with retinal degeneration (P90-140,  $n = 5$ ; p300-400,  $n = 2$ ) from a Royal College of  
16 Surgeons (RCS) colony maintained at the Stanford Animal facility. Female Long-Evans adult WT rats  
17 ( $n = 4$ ) were purchased from Charles River (Wilmington, MA, USA). All animals were housed in a 12-h  
18 light/12-h dark cycle with food and water ad libitum. We conducted all experimental procedures in  
19 accordance with the Stanford University and University of California Santa Cruz institutional  
20 guidelines, and conformed to the guidelines of the Association for Research in Vision and  
21 Ophthalmology (ARVO) Statement for the Use of Animals in Ophthalmic and Vision research.

22 The animals were euthanized (390 mg/ml pentobarbital sodium, 50 mg/ml phenytoin sodium)  
23 before one eye was enucleated. We isolated a small piece of retina ( $\sim 3 \times 3 \text{mm}$ ) and placed it on the  
24 512-electrode recording array<sup>16</sup> ganglion cell side down. We recorded from one piece of retina per  
25 animal. The photovoltaic array was then placed on top of the retina, simulating a subretinal

1 placement *in-vivo*<sup>7</sup>. We ensured good contact between the retina and the stimulating and recording  
2 arrays by carefully pressing down on the implant with a plastic mesh. We perfused the retina with  
3 Ames solution (Sigma-Aldrich) saturated in oxygen and kept at 27°C. Voltage waveforms were  
4 sampled and recorded at 20kHz on each of the 512 electrodes of the recording array<sup>16</sup>.

### 5 ***Visual stimulation***

6 For evaluation of prosthesis-mediated vision, we activated the photovoltaic array using a near-  
7 infrared (NIR) projection system, which consisted of a polarization-scrambled array of NIR (880 nm)  
8 laser diodes coupled into a 400  $\mu\text{m}$  multimode fiber (Dilas M1F4S22-880.3-30C-SS2.1). We  
9 collimated the laser beam at the output of the fiber and used a 2° divergence microlens array diffuser  
10 to improve beam homogeneity. The beam was projected onto the implant via the camera port of an  
11 inverted microscope (Olympus IX-71, 5x objective). We controlled the timing, width and amplitude of  
12 the light using a National Instruments USB-6353 data acquisition card and custom software.

13 For evaluation of the natural responses to visible light, we projected the optically minified image of a  
14 15" CRT screen (model Sony CPD-E100) on the photoreceptor layer of a healthy retina through the  
15 camera port of the inverted microscope. We modulated the light intensity over the full field using  
16 randomized light pulses drawn so as to keep a mean luminance level corresponding to 0.5 of the  
17 maximum brightness over the duration of the stimulus. The light flux at the 0.5 gray background level  
18 was equivalent to 19,000 photons/ $\mu\text{m}^2/\text{s}$  produced by a monochromatic source of wavelength 515  
19 nm. Each intensity step lasted 0.5 second before a 0.5 second-long step to the following intensity (Fig.  
20 1A). We kept intensities between the  $0.5-0.48 = 0.02$  and  $0.5+0.48 = 0.98$  levels, which correspond to  
21 the limits of the range of intensities over which we are able to modulate the pixels intensity on the  
22 CRT linearly. We used  $n = 100$  trials for each intensity value in order to detect deviations from the  
23 spontaneous firing rate that are half its standard deviation or larger, with a  $P$  value of 0.01 and a  
24 statistical power of 0.8, for which a minimum of  $n = 94$  trials is required<sup>17</sup>.

25 For evaluation of responses to prosthetic stimulation, we used a carrier waveform consisting of 20  
26 Hz, 4 ms pulses of NIR light. We modulated the envelope of the carrier waveform using a square wave  
27 consisting of a 0.5 second-long maximum value of 2.5 mW/ $\text{mm}^2$  (140 $\mu\text{m}$  pixels) or 5mW/ $\text{mm}^2$  (70 $\mu\text{m}$

1 pixels) followed by a 0.5 second-long OFF value randomly selected from a pre-determined list of  
2 values between 0 and the maximum intensity (Fig. 1B). We used  $n = 150$  trials for each intensity  
3 value, in order to maintain adequate statistical power with increased noise levels due to electrical  
4 stimulation.

5 In addition to full-field light intensity steps, we stimulated the WT retinas with a spatio-temporal  
6 white noise, which allowed us to calculate spike triggered average (STA) response of the detected  
7 RGCs<sup>18</sup>. Time dependence of the calculated STAs was used to classify cells into ON-center and OFF-  
8 center types<sup>19</sup>. The spatiotemporal monochromatic white noise stimulus consisted of 100 x 60  
9 square pixels with each pixel 70  $\mu\text{m}$  on a side, refreshed every 33.33 ms. We randomly set the  
10 relative intensity level for each pixel in each frame above or below the 0.5 mean background level at  
11  $0.5 \pm 0.48$ . The corresponding contrast,  $(I_{\text{max}} - I_{\text{min}})/(I_{\text{max}} + I_{\text{min}})$ , was therefore 96%, where  $I_{\text{max}}$  and  
12  $I_{\text{min}}$  are the maximum and minimum intensities, respectively.

### 13 ***Data analysis***

14 For prosthetic stimulation data, we initially subtracted stimulation artifacts from the raw voltage  
15 traces recorded on the electrode array and subsequently analyzed the data using custom-written  
16 software<sup>16</sup>. We estimated electrical stimulation artifacts by averaging their shape over many (100+)  
17 trials. The average artifact shape was subsequently aligned to the raw recordings and pointwise  
18 subtracted from them. This method was sufficient for removal of the artifact immediately following  
19 the pulse, but often insufficient for the artifact removal during the light pulse, therefore we blanked  
20 this phase during processing of the recordings (Fig 1C-D). As a consequence, all possible direct  
21 stimulation of the RGCs (latency  $\leq 1\text{ms}$ <sup>20</sup>) was ignored in our analysis.

22 We performed action potential detection by thresholding the artifact-removed data. All action  
23 potential waveforms were aligned to the time of maximum deflection from baseline, and we  
24 performed dimensionality reduction on the waveforms by principal component analysis, prior to  
25 expectation-maximization clustering<sup>16, 21</sup>. For each putative neuron, we calculated the  
26 electrophysiological image (EI) of the neuron, i.e. the average voltage waveform recorded on the  
27 whole multielectrode array when the neuron produced an action potential<sup>22-24</sup>. We discarded

1 neurons exhibiting abnormal EIs from the analysis, as well as neurons for which violations of the  
 2 refractory period occurred within the action potential train. Finally, we removed neurons with the  
 3 same EI from the analysis, as they correspond to redundant detections of a single neuron over  
 4 multiple electrodes, and only the putative neuron with the largest action potential count was kept.  
 5 The neuron selection process is described in more details in the literature<sup>7, 11</sup>.

6 For each contrast step, we constructed peristimulus time histograms (PSTHs) by binning action  
 7 potentials over 5 ms periods and averaging over 100 (visible) or 150 (prosthesis) trials. We used the  
 8 Michelson definition for contrast  $(I_{\text{post}} - I_{\text{pre}})/(I_{\text{post}} + I_{\text{pre}})$ , where  $I_{\text{pre}}$  is the luminance (or peak  
 9 intensity for prosthetic stimulation) pre contrast step and  $I_{\text{post}}$  is the luminance post contrast step.  
 10 We defined the steady-state retinal activity as the firing rate over the 300-500 ms period post-  
 11 stimulus. For visible light stimulation, we compared the steady-state activity to the activity in the 50-  
 12 150 ms following each contrast step. The amplitude of the response was quantified as the positive  
 13 variation from steady-state activity in number of action potentials. For prosthetic stimulation, latency  
 14 of the elicited action potentials was shorter than for visual stimulation<sup>7</sup>, likely because electrical  
 15 stimulation bypasses the slow phototransduction cascade. Therefore, steady-state activity was  
 16 compared to the activity in the 5-100 ms following each contrast step. All neurons that did not  
 17 respond to at least one value of contrast change with an average of 0.5 action potential elicited per  
 18 trial were considered non-responsive and were discarded from the analysis. We included in the  
 19 analysis the experimental preparations in which at least 10 RGCs underneath the implant responded  
 20 to 100% contrast steps over the full-field.

21 For each neuron, we plotted the number of elicited action potentials vs. amplitude of the contrast  
 22 step and fitted the resulting curves with two generalized sigmoid functions, one for the OFF  
 23 component of the response and the other for the ON component, such that:

$$\begin{cases} r = f(\log -c, \tau_l, \mu_l, \sigma_l, \rho_l) & \text{if } c < 0 \\ r = 0 & \text{if } c = 0 \\ r = f(\log c, \tau_r, \mu_r, \sigma_r, \rho_r) & \text{if } c > 0 \end{cases}$$

24 where  $f(x, \tau, \mu, \sigma, \rho) = \tau \left(1 + e^{-(x-\mu)/\sigma}\right)^{-\rho}$ ,  $c$  is the contrast and  $r$  the response of the neuron.

1 We defined the stimulation threshold as a 50% probability of eliciting an action potential, as  
2 estimated from the generalized sigmoid fit. We classified neurons that responded primarily to  
3 luminance increments with prosthetic stimulation as electrical ON cells, neurons that responded  
4 primarily to luminance decrements as electrical OFF cells and neurons that responded to both  
5 luminance increments and decrements as eON-OFF cells. The classification was based on three  
6 ranges of the ratio of  $\max(\text{ON response})/\max(\text{OFF response})$ :  $<1/3$  – eOFF,  $[1/3, 3]$  – eON-OFF and  
7  $>3$  – eON.

## 8 **Results**

### 9 ***RGC responses to contrast steps***

10 In normal retina, visual information is transduced by the photoreceptors, further processed in the  
11 inner nuclear layer and ultimately transmitted to the RGCs, which relay it to the brain. The receptive  
12 fields of different RGC types form complementary mosaics over the retinal surface<sup>19, 25-28</sup>. Very  
13 generally, RGCs respond to changes in luminance by generating action potentials in response to light  
14 increments (ON- cells), or decrements (OFF- cells), or both increments and decrements in  
15 illumination (ON-OFF cells)<sup>29</sup>. In this study we did not classify RGCs by their direction-of-motion or  
16 object-motion selectivity<sup>30, 31</sup>.

17 To measure contrast sensitivity of the healthy (wild-type, Long Evans, WT) rat retina, we projected  
18 full-field visible light steps of varying amplitude on the photoreceptor layer. We projected similar  
19 patterns on a photovoltaic implant pressed on the photoreceptor side of WT and degenerate (Royal  
20 College of Surgeons, RCS) rat retina using high frequency near infrared (NIR) illumination (Methods  
21 and Fig. 1). We recorded from  $n = 360$  neurons for visible light stimulation of the WT retina,  $n = 75$   
22 neurons for prosthetic stimulation of the WT retina,  $n = 91$  neurons for prosthetic stimulation of the  
23 P90-140 RCS retina using  $70\ \mu\text{m}$  pixel size implants,  $n = 65$  neurons for prosthetic stimulation of the  
24 P90-140 RCS retina using  $140\ \mu\text{m}$  pixel size implants and  $n = 28$  neurons for prosthetic stimulation of  
25 the P300-400 RCS retina using  $140\ \mu\text{m}$  pixel size implants. Responses to both visible light stimulation  
26 and near-infrared stimulation could be classified as ON, OFF or ON-OFF (Methods and Fig. 2). We will

1 denote visible light responses as vON (Fig. 2B), vON-OFF (Fig. 2C) and vOFF (Fig. 2D) in the rest of  
2 the text in order to distinguish them from their prosthetic counterparts, electrical eON (Fig. 2E), eON-  
3 OFF (Fig. 2F) and rare, weak eOFF (Fig. 2G,  $n = 9/75$  neurons for WT retina and  $n = 2/184$  neurons  
4 for RCS retina).

5 Responses to prosthetic stimulation exhibited shorter latencies than responses to visible light  
6 (typical latency of 5-100ms following the contrast step, as compared to latencies of 50-150ms for  
7 visible light stimulation), likely because prosthetic stimulation bypasses the slow phototransduction  
8 cascade<sup>7</sup>. The ratio of prosthetic stimulation thresholds between ON-center and OFF-RGCs in WT  
9 retinas was  $1.24 \pm 0.31$  (mean  $\pm$  SEM), not substantially different between the two cell classes.

10 The proportion of eON, eOFF and eON-OFF responses varied significantly between healthy and  
11 degenerate animals as well as between RCS animals at different stages of degeneration. For WT  
12 animals, purely eON responses accounted for 32% of the responsive neurons we recorded from. For  
13 p90-140 RCS animals, this fraction went up to 68% and for p300-400 animals, 89% of the responses  
14 to electrical stimulation did not have any OFF component anymore (Table 1). In the WT retina,  
15 among OFF-center RGCs (identified from a binary white noise stimulus, Methods), 56% responded as  
16 purely eON, while 22% responded as eON-OFF and 22% as eOFF cells. ON-center RGCs responded  
17 primarily (83%) as eON-OFF cells, with another 14% responding as eON cells and the other 3%  
18 responding as eOFF cells (Table 2).

19 The reduction in the fraction of eOFF responses with time indicates photoreceptor involvement in  
20 their generation. Histological analysis of the WT and RCS retina (Fig. 3) reveals that while the  
21 photoreceptor outer segments have degenerated by P90 in the RCS retina, a significant fraction of the  
22 photoreceptor somas remain, which could account for the remaining eOFF responses at P90. At P400,  
23 the photoreceptor somas are virtually all gone, as is the eOFF component of the response.

#### 24 ***Contrast sensitivity of the retinal response to prosthetic stimulation***

25 Plotting the mean population response to contrast steps (Fig. 4) reveals two striking features of  
26 prosthetic vision, compared to natural light responses: (a) dynamic range of the responses is



1 considerably reduced and (b) very large contrast steps are required to elicit reliable responses in the  
2 RGCs.

3 We defined stimulation thresholds as a 50% probability of eliciting an action potential<sup>7, 11, 32, 33</sup>  
4 (Methods). For visible light stimulation, the mean stimulation threshold was 7% positive contrast for  
5 vON cells, and 3% negative contrast for vOFF cells. When stimulating p90-140 and p300-400 RCS  
6 retina with either 70 $\mu$ m or 140 $\mu$ m pixel size implants, stimulation threshold was measured to be  
7 between 56% (p300-400 RCS retina, 140 $\mu$ m pixels) and 70% (p90-140 RCS retina, 140 $\mu$ m pixels)  
8 contrast. Maximum amplitude of the response was on average 3.6 action potentials per contrast step  
9 for vON responses of the WT retina and 7.2 action potentials per contrast step for vOFF responses  
10 (Fig. 4A). Amplitude of the response was significantly reduced with prosthetic stimulation of  
11 degenerate tissue, with only 1.2 action potentials per contrast step for stimulation of p90-140 RCS, in  
12 the eON response. Since eOFF and eON-OFF responses in degenerate tissue largely disappear at the  
13 later phases of degeneration, we will ignore the few neurons that were detected as eOFF or eON-OFF  
14 in RCS tissue in further analysis.

15 We did not observe a significant change in contrast sensitivity thresholds or amplitude of the  
16 response of RCS retina to prosthetic stimulation with age (Fig. 4C, D;  $P = 0.21$  and  $P = 0.27$  for a  
17 change in contrast sensitivity and amplitude, respectively, two-sample KS test), or with the size of the  
18 stimulating pixel (Fig. 4B, C;  $P = 0.66$ , two-sample KS test): 1.2 action potentials were elicited per  
19 contrast step in p90-140 RCS retina with both 70 and 140 $\mu$ m pixels, and 1.5 action potentials elicited  
20 in p300-400 RCS retina with 140 $\mu$ m pixels. This result suggests that while pixel size affects  
21 stimulation thresholds<sup>8, 34</sup>, it might not influence significantly the contrast sensitivity once the  
22 irradiance is modulated around a constant adaptation level far above stimulation threshold.

### 23 ***Delivering visual information with a subretinal prosthesis***

24 Visual perception of brightness is determined primarily by local spatio-temporal contrast of the  
25 visual stimulus<sup>13, 35, 36</sup>. During visual fixation of a static scene, the retina locally adapts to the average  
26 luminance over the course of a few hundred milliseconds<sup>37</sup>. RGCs then respond to local changes in  
27 contrast triggered by ocular movements such as microsaccades, drift and ocular tremor. It has been

1 hypothesized that ocular movements prevent perceptual fading by continuously stimulating neurons  
2 that respond transiently to stimuli<sup>38</sup> and contribute to encoding of visual scenes<sup>13</sup>.

3 Fixational eye movements (FEMs) transform static spatial modulation in luminance in images into  
4 temporal modulation of luminance on the retina. Recent studies<sup>12, 13</sup> have shown that the statistical  
5 properties of FEMs are well tuned to the statistics of natural scenes and perform whitening of spatial  
6 frequencies below 30 cycles per degree – the resolution limit of a typical human eye. Contrast  
7 sensitivities of RGCs are, in turn, well adapted to the resulting spatio-temporal patterns of light on  
8 the retina, producing robust RGC responses. Prosthetic vision exhibits much lower full-field contrast  
9 sensitivity and a lack of OFF responses, which is likely to disrupt these finely tuned fixational  
10 mechanisms.

11 To illustrate the effect of reduced contrast sensitivity on the ability of the retina to encode visual  
12 information, we considered a 1-dimensional step in intensity (Figure 5A, top panel) and estimated  
13 the contrast between the light pattern and the static component of the retinal image caused by visual  
14 fixation<sup>12</sup>. This static component, the local average luminance, was obtained by convolution of the  
15 light step with a blurring kernel defined by the distribution of eye movements (Figure 5A, middle  
16 panel). The underlying assumption is that the amplitude of FEMs determines the spatial scale over  
17 which the average luminance on the retina is determined. Amplitude of the blurring kernel decreases  
18 proportionally to one minus the cumulative distribution function of microsaccades<sup>39</sup> and the  
19 probability distribution function of microsaccade amplitude is modeled as a gamma distribution,  
20 with shape parameter 2 and scale parameter  $0.15^\circ$ .

21 The maximum positive contrast between a step pattern and its local average luminance is  $1/3$ ,  
22 independently of the width of the blurring kernel (Figure 5A, lower panel), much lower than the  
23 contrast stimulation threshold with prosthetic vision. Large lateral displacements of the pattern – on  
24 the order of the size of the blurring kernel – are required to cause a 60% change in local contrast. In  
25 other words, only large and rare microsaccadic eye movements can trigger a sufficient change in  
26 luminance for eliciting retinal activity.

1 To guarantee that any displacement of the image will trigger an ON response in a system with  
2 contrast sensitivity  $c$ , a binary image should be at least locally  $x$ -sparse, where  $x = (1-c)/(1+c)$  on the  
3 spatial scale of the luminance averaging. In the 1-dimensional case, a thin line meets this criterion  
4 (Figure 5B), so any small displacement of the pattern can introduce sufficient changes in the local  
5 contrast to trigger a response. For prosthetic vision with contrast sensitivity thresholds around 60%,  
6 this criterion means that binary images should be at least locally 25% sparse to efficiently deliver  
7 visual information. The more images deviate from this criterion, the less retinal activity will be  
8 elicited by the temporal changes in luminance produced by FEMs.

9 Most static visual scenes in general, and natural scenes in particular, fail to meet such a local sparsity  
10 constraint. We exemplified this by simulating the response of prosthetic vision to natural images  
11 (Figure 6) using a convolutional linear-nonlinear (LN) model of RGCs<sup>40, 41</sup>. After blurring the image by  
12 convolution with the eye movement kernel (second column in Figure 6), we calculated the contrast  
13 between the static component of the retinal image and the natural scene (Figure 6, third column).  
14 Previously experimentally measured contrast sensitivity curves were used to convert the local  
15 contrast into RGC firing rates (Figure 6, fourth column). With a complete characterization of the  
16 spatial dependence of contrast sensitivity of prosthetic vision, this model could be expanded to take  
17 into account the multiple spatial scales present in visual scenes and could lead to more accurate  
18 predictions.

19 For simulation of normal vision, we used an image with the spatial resolution of the fovea (5 $\mu$ m pixel  
20 pitch on the retina, Figure 6A). For simulation of prosthetic responses, images were first down-  
21 sampled by the pixel size in order to reflect the expected spatial resolution of the implant<sup>11</sup>.

22 Therefore, we used a 50 $\mu$ m and a 150 $\mu$ m square lattice sampling density and contrast sensitivity  
23 curves as measured with the prosthesis (Figure 6 B and C). In the case of natural vision, this simple  
24 model predicts strong responses localized, as expected, around the edges and textured areas.

25 However, in the case of prosthetic vision, it predicts an almost no responses due to its poor contrast  
26 sensitivity to ON stimulation and lack of OFF responses.

## 27 **Discussion**

1 Bypassing the photoreceptors with subretinal electrical stimulation has strong implications on  
2 contrast sensitivity and dynamic range of prosthetic vision. Light stimulation of the photoreceptors  
3 leverages a finely tuned amplification cascade that can trigger responses to very dim illumination (a  
4 few photons only, <sup>42,43</sup>), or to minute changes in contrast<sup>44</sup>. Prosthetic subretinal stimulation of the  
5 inner nuclear layer in the degenerate retina elicits responses with, at best, twice smaller amplitude  
6 and ten times lower contrast sensitivity than normal.

7 While electrical stimulation of the healthy retina exhibits at least three types of responses to contrast  
8 steps (eON, eOFF and eON-OFF), the eOFF component can be explained by electrical stimulation of  
9 the photoreceptor layer. If only photoreceptors, bipolar and retinal ganglion cells were involved in  
10 the response to full-field contrast steps, electrical stimulation of the photoreceptors should  
11 depolarize them, thereby triggering action potentials and therefore apparent ON response in the OFF  
12 pathway at the onset of electrical stimulation. When electrical stimulation stops, the photoreceptors  
13 should hyperpolarize again, causing an electrical OFF response in the ON pathway this time. With  
14 full-field stimulation of the rat retina, additional amacrine cell-mediated network effects further  
15 complicate the response. This makes it difficult to pharmacologically dissect the mechanisms behind  
16 the electrical OFF response. However, its progressive and almost complete disappearance with  
17 advancing degeneration, correlated with disappearance of the photoreceptors in the RCS retina,  
18 strongly indicates that it is indeed mediated by photoreceptors.

19 We did not observe a difference in contrast sensitivity between implants with 70 $\mu$ m and 140 $\mu$ m  
20 pixels, indicative that while stimulation thresholds are affected by pixel size<sup>8,34</sup>, the contrast  
21 sensitivity function itself does not change once the retina adapts to above-threshold stimulation  
22 levels at high frequency (>20Hz). The contrast sensitivity we measured matches values previously  
23 observed in-vivo<sup>34</sup>, and, importantly, it did not decline with age of the degenerate retinas (p90-140  
24 vs. p300-400) despite the expected changes in the retinal network<sup>45</sup>.

25 Subretinal stimulation preserves a few important features of retinal signal processing, such as flicker  
26 fusion and transient responses to slower changes in luminance, as well as non-linear integration  
27 across subunits of RGCs with large receptive fields<sup>11</sup>. However, disappearance of the electrical OFF

1 responses means that both the ON and OFF pathways are activated simultaneously, a very unnatural  
2 stimulation paradigm. Indiscriminate activation of all the cells in the inner nuclear layer is likely to  
3 contribute to reduced contrast sensitivity since both excitatory bipolar and inhibitory amacrine cells  
4 could be driven by the prosthesis. It remains unclear how this phenomenon affects phosphene  
5 perception, since current clinical trials with subretinal prosthesis demonstrated that patients see  
6 phosphenes primarily as light rather than dark flashes, and can perceive patterns of stimulation<sup>14</sup>.

7 The full-field measurements of contrast sensitivity we conducted do not take into account contrast  
8 improvements at higher spatial frequencies due to center-surround effects in normal vision<sup>46</sup>. It is  
9 reasonable to expect this effect to be less pronounced with a subretinal prosthesis than with normal  
10 vision since horizontal cells responsible for part of the center-surround effects in the retina are  
11 thought to only synapse directly onto photoreceptors which disappear with degeneration, and not  
12 bipolar cells<sup>47</sup>. Therefore, only lateral inhibition from the amacrine cells should be able to contribute  
13 to center-surround effects with subretinal prosthetic stimulation.

14 Contrast sensitivity of the system with patterned stimulation<sup>48, Loudin2007</sup> is also strongly affected by  
15 configuration of the return electrodes, and implants with distant returns exhibit significantly lower  
16 electrical contrasts as compared to implants with local returns, such as those used in this study.

17 Making predictions about the human visual system based on measurements with a degenerate rat  
18 retina is difficult, given the major differences between the visual systems of the two species. The  
19 midget, parasol and small bistratified cells that dominate the human visual pathways<sup>49</sup> have no  
20 anatomical equivalence in rat. It is possible that the magnocellular-projecting parasol cells would  
21 have higher contrast sensitivities than the values we observed in rats. In addition, differences in the  
22 rate and extent of retinal degeneration between humans and various animal models make it even  
23 more difficult to predict responses to electrical stimulation in human patients.

24 An important consequence of the reduced contrast sensitivity and lack of OFF responses with  
25 prosthetic vision is that efficiency of fixational eye movements for image refreshing and prevention  
26 of perceptual fading<sup>13, 38</sup> is greatly diminished, compared to natural vision. While it is possible to  
27 deliver information with relatively high spatial content through the implant<sup>11</sup>, most static visual

1 scenes are not sparse enough to elicit responses in RGCs with FEMs alone. This phenomenon could  
2 be responsible for the perceptual fading at high stimulation frequencies reported in patients with the  
3 subretinal implant Alpha-IMS, when FEMs which appear normal with the implant turned on<sup>50</sup> would  
4 be expected to trigger retinal responses. Patients prefer stimulation frequencies not exceeding 7 Hz<sup>50</sup>,  
5 <sup>51</sup> – well below the flicker fusion frequency, so the pulses introduce strong temporal contrast in the  
6 visual pattern. Lack of contrast sensitivity appears to be an important limitation of subretinal  
7 prosthetic devices that can strongly impede their ability to deliver visual information efficiently to  
8 the brain. This could be partially mitigated by pre-processing of the images between the camera and  
9 the implant, which by increasing local image sparsity could bring local contrast above stimulation  
10 thresholds.

## 11 **Acknowledgements**

12 We would like to thank Prof. E.J. Chichilnisky, M. Marmor, Drs. D. Boinagrov and H. Lorach for  
13 stimulating discussions. We are grateful to Prof. A. Litke, P. Hottowy, S. Kachiguine and P. Hausser for  
14 providing access to and support of the multielectrode array recording setup. We would like to thank  
15 Dr. H. Lorach, R. Dalal and P. Huie for their help with histological images.

16

## 1 **Figures and tables**

2 Figure 1: **Stimulation protocol.** (A) With visible illumination, contrast steps are presented using  
3 continuous illumination. (B) Prosthetic stimulation consists of contrast steps with the same envelope  
4 modulating a 20Hz train of near-infrared pulses. (C), (D) Voltage traces from two different  
5 electrodes. Note that the periodic “quiet” regions in these traces coincide with the removed  
6 stimulation artifacts during which information about the waveform was lost due to amplifier  
7 saturation. (C) Two neurons were detected on this electrode, one of which (larger amplitude action  
8 potentials) responded transiently to the positive contrast step while the other (smaller action  
9 potentials) did not respond to stimulation. (D) On this electrode, neurons transiently respond both to  
10 the positive and the negative contrast steps.

11

12 Figure 2: **Single-unit responses to contrast steps.** (B) vON, (C) vON-OFF and (D) vOFF responses to (A)  
13 full-field contrast steps observed with visible light in the WT retina. Neurons responded to both high  
14 and low contrast steps. Similar (E) eON, (F) eON-OFF and weak (G) eOFF responses observed with  
15 electrical stimulation in the degenerate RCS retina. With electrical stimulation, neurons did not  
16 respond to lower contrast steps. The periodic gaps in the histograms are due to electrical stimulation  
17 artifacts, which prevent detection of action potentials during the stimulation pulses.

18

19 Figure 3: **Histological analysis of the RCS rat retina.** (A) In the healthy WT retina, photoreceptor outer  
20 segments (OS) transduce light and modulate the membrane potential of photoreceptor somas located  
21 in the outer nuclear layer (ONL). Photoreceptors transmit neural information to cells in the inner  
22 nuclear layer (INL), which then relay it to the ganglion cells (GCL). (B) In the P90 RCS retina, the  
23 outer segments have been replaced by debris, and only a fraction of the photoreceptors somas  
24 remain in the INL. (C) At P400, all the photoreceptor somas are gone from the RCS retina and only  
25 the INL and GCL remain. Scale bar: 50µm.

26

1 Figure 4: **Mean population responses to contrast steps.** (A) WT responses to visible full field light steps  
2 could broadly be classified into vON (red), vOFF (blue) and vON-OFF (purple) responses. The black  
3 dashed line outlines the stimulation threshold, defined as a 50% probability of eliciting an action  
4 potential correlated with the contrast step. On average, ON cells responded to contrast increments  
5 greater than 7%, while OFF cells responded to contrast decrements as small as 3%. (B) Photovoltaic  
6 stimulation of p90-140 RCS retina with 70 $\mu$ m pixel implants requires 67% contrast steps to elicit  
7 responses in the RGCs. Maximum amplitude of the response is lower than with visible light in the WT  
8 retina. Contrast sensitivity curves are very similar with (C) 140 $\mu$ m pixels used to stimulate p90-140  
9 RCS retina and (D) in advanced stages of retinal degeneration (p300-400 RCS rats). Confidence band  
10 represents the standard error of the mean.

11

12 Figure 5: **Effect of reduced contrast sensitivity on perception of 1-dimensional patterns.** The average  
13 local luminance is estimated by convolving the light pattern (top row) with a blurring kernel defined  
14 by the distribution of eye movements (middle row). The resulting local contrast is estimated and  
15 compared to full-field contrast stimulation thresholds (bottom row). Red shaded area: above  
16 threshold for prosthetic stimulation; blue shaded area: above threshold for visible light stimulation.  
17 (A) In the case of a step, the local contrast between the image and the average local luminance is  
18 below the threshold for infinitesimal eye movements (solid green line). Only large displacements of  
19 the visual scene will result in a sufficiently large contrast between the average local luminance and  
20 the visual scene to trigger responses (dashed green line, corresponding to a 90  $\mu$ m lateral  
21 displacement also indicated on the blurring kernel). (B) In the case of a line, the pattern is sparse  
22 enough to provide contrast exceeding stimulation threshold for both natural and prosthetic vision  
23 even with small image displacements.

24

25 Figure 6: **Prosthetic response to a natural scene.** (A) Local contrast changes in a natural scene are large  
26 enough to elicit robust RGC responses with normal vision. With prosthetic stimulation they are  
27 insufficient to enable image refresh through microsaccades for implants with both (B) 50 $\mu$ m pixels  
28 and (C) 150 $\mu$ m pixels.



1 **Tables**

2

	WT	RCS, p90-140	RCS, p300-400
<b>eON</b>	32%	68%	89%
<b>eON-OFF</b>	56%	30%	7%
<b>eOFF</b>	12%	2%	4%
<b>Cell count</b>	75	156	28

3

Table 1: Prevalence of eON, eOFF and eON-OFF responses in different animal models.

4

	OFF-center	ON-center
<b>eON</b>	56%	14%
<b>eON-OFF</b>	22%	83%
<b>eOFF</b>	22%	3%

5

Table 2: Mapping visible light responses to prosthetic responses.

6

7

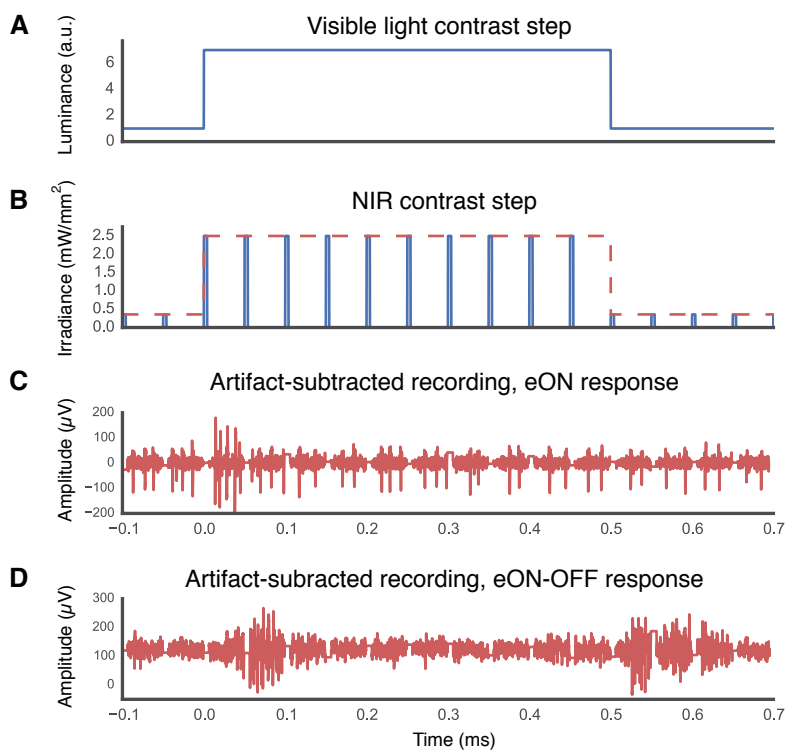
## References

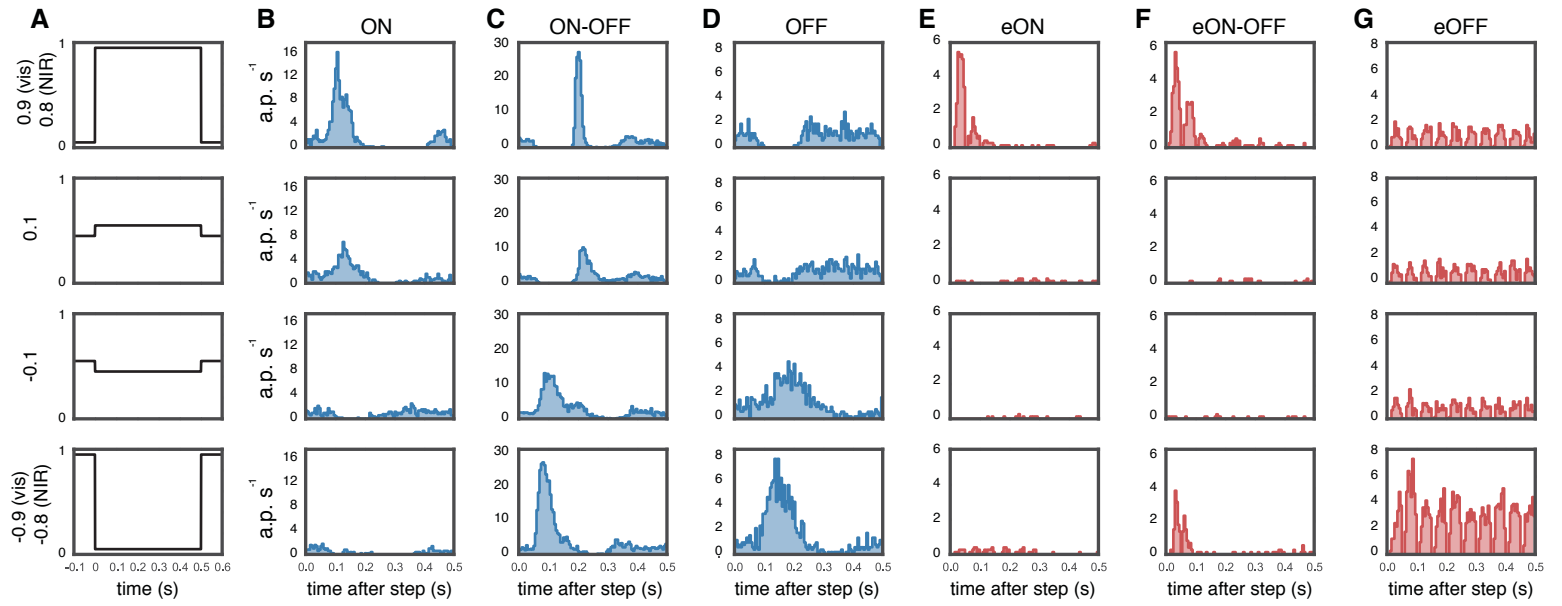
1. Smith W, Assink J, Klein R, et al. Risk factors for age-related macular degeneration: Pooled findings from three continents. *Ophthalmology* 2001;108:697-704.
2. Mazzoni F, Novelli E, Strettoi E. Retinal ganglion cells survive and maintain normal dendritic morphology in a mouse model of inherited photoreceptor degeneration. *J Neurosci* 2008;28:14282-14292.
3. Humayun MS, Prince M, de Juan E, et al. Morphometric analysis of the extramacular retina from postmortem eyes with retinitis pigmentosa. *Invest Ophthalmol Vis Sci* 1999;40:143-148.
4. Kim SY, Sadda S, Pearlman J, et al. Morphometric analysis of the macula in eyes with disciform age-related macular degeneration. *Retina* 2002;22:471-477.
5. Marc RE, Jones BW. Retinal Remodeling in Inherited Photoreceptor Degenerations. *Molecular Neurobiology* 2003;28:139-147.
6. Jensen RJ, Rizzo JF. Thresholds for activation of rabbit retinal ganglion cells with a subretinal electrode. *Experimental eye research* 2006;83:367-373.
7. Mathieson K, Loudin J, Goetz G, et al. Photovoltaic Retinal Prosthesis with High Pixel Density. *Nat Photonics* 2012;6:391-397.
8. Mandel Y, Goetz G, Lavinsky D, et al. Cortical responses elicited by photovoltaic subretinal prostheses exhibit similarities to visually evoked potentials. *Nat Commun* 2013;4:1980.
9. Goetz GA, Mandel Y, Manivanh R, Palanker DV, Cizmar T. Holographic display system for restoration of sight to the blind. *Journal of neural engineering* 2013;10:056021.
10. Boinagrov D, Lei X, Goetz G, et al. Photovoltaic Pixels for Neural Stimulation: Circuit Models and Performance. *IEEE Trans Biomed Circuits Syst* 2015.
11. Lorach H, Goetz G, Smith R, et al. Photovoltaic restoration of sight with high visual acuity. *Nature Medicine* 2015;in print.
12. Kuang X, Poletti M, Victor JD, Rucci M. Temporal encoding of spatial information during active visual fixation. *Curr Biol* 2012;22:510-514.
13. Rucci M, Victor JD. The unsteady eye: an information-processing stage, not a bug. *Trends Neurosci* 2015;38:195-206.
14. Stingl K, Bartz-Schmidt K-U, Gekeler F, Kusnyerik A, Sachs H, Zrenner E. Functional Outcome in Subretinal Electronic Implants Depends on Foveal Eccentricity. *Investigative Ophthalmology & Visual Science* 2013;54:7658-7665.
15. Wang L, Mathieson K, Kamins TI, et al. Photovoltaic retinal prosthesis: implant fabrication and performance. *Journal of neural engineering* 2012;9:046014.
16. Litke AM, Bezayiff N, Chichilnisky EJ, et al. What Does the Eye Tell the Brain? Development of a System for the Large-Scale Recording of Retinal Output Activity. *IEEE Trans on Nuclear Science* 2004;51:1434-1440.
17. Whitley E, Ball J. Statistics review 4: Sample size calculations. *Crit Care* 2002;6:335-341.
18. Chichilnisky EJ. A simple white noise analysis of neuronal light responses. *Network: Comput Neural Syst* 2001;12:199-213.

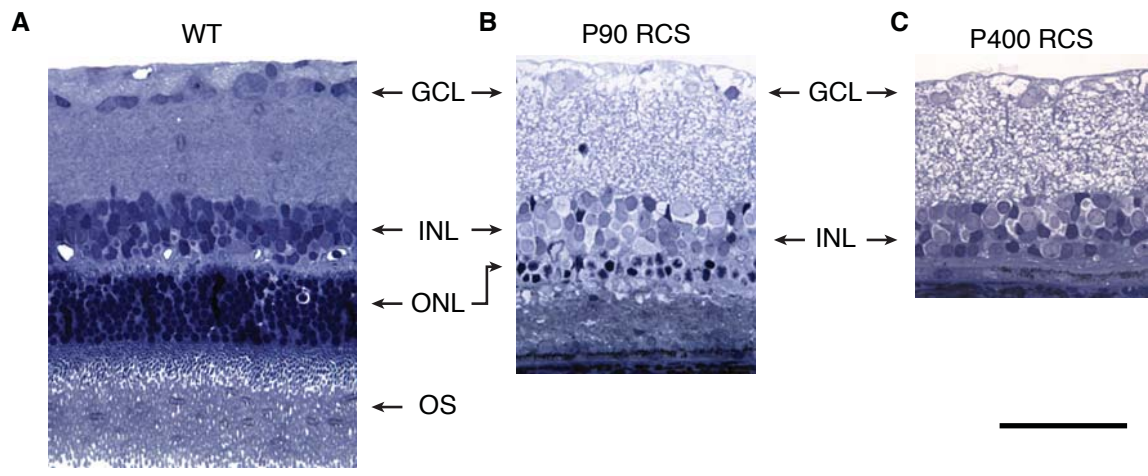
- 1 19. Chichilnisky EJ, Kalmar RS. Functional Asymmetries in ON and OFF Ganglion  
2 Cells of Primate Retina. *The Journal of Neuroscience* 2002;22:2737-2747.
- 3 20. Boinagrov D, Pangratz-Fuehrer S, Goetz G, Palanker D. Selectivity of Direct and  
4 Network-mediated Stimulation of the Retinal Ganglion Cells with Epi-, Sub-  
5 and Intra-Retinal Electrodes. *Journal of neural engineering* 2014;11:026008.
- 6 21. Lewicki MS. A review of methods for spike sorting: the detection and  
7 classification of neural action potentials. *Network: Comput Neural Syst*  
8 1998;9:R53-R78.
- 9 22. Petrusca D, Grivich MI, Sher A, et al. Identification and characterization of a Y-  
10 like primate retinal ganglion cell type. *The Journal of neuroscience : the official*  
11 *journal of the Society for Neuroscience* 2007;27:11019-11027.
- 12 23. Greschner M, Field GD, Li PH, et al. A polyaxonal amacrine cell population in  
13 the primate retina. *The Journal of neuroscience : the official journal of the*  
14 *Society for Neuroscience* 2014;34:3597-3606.
- 15 24. Li PH, Gauthier JL, Schiff ML, et al. Anatomical Identification of Extracellularly  
16 Recorded Cells in Large-Scale Multielectrode Recordings. *J Neurosci*  
17 2015;31:xxxx-xxxx.
- 18 25. Devries SH, Baylor DA. Mosaic Arrangement of Ganglion Cell Receptive Fields  
19 in Rabbit Retina. *Journal of neurophysiology* 1997;78:2048-2060.
- 20 26. Field GD, Sher A, Gauthier JL, et al. Spatial properties and functional  
21 organization of small bistratified ganglion cells in primate retina. *The Journal of*  
22 *neuroscience : the official journal of the Society for Neuroscience*  
23 2007;27:13261-13272.
- 24 27. Dacey DM, Petersen MR. Dendritic field size and morphology of midget and  
25 parasol cells of the human retina. *PNAS* 1992;89:9666-9670.
- 26 28. Wassle H. Parallel processing in the mammalian retina. *Nat Rev Neurosci*  
27 2004;5:747-757.
- 28 29. Heine WF, Passaglia CL. Spatial receptive field properties of rat retinal ganglion  
29 cells. *Visual Neuroscience* 2011;28:403-417.
- 30 30. Borst A, Euler T. Seeing things in motion: models, circuits, and mechanisms.  
31 *Neuron* 2011;71:974-994.
- 32 31. Olveczky BP, Baccus S, Meister M. Segregation of object and background  
33 motion in the retina. *Nature* 2003;423:401-408.
- 34 32. Sekirnjak C, Hottowy P, Sher A, Dabrowski W, Litke AM, Chichilnisky EJ.  
35 Electrical stimulation of mammalian retinal ganglion cells with multielectrode  
36 arrays. *Journal of neurophysiology* 2006;95:3311-3327.
- 37 33. Jepson LH, Hottowy P, Mathieson K, et al. Focal electrical stimulation of major  
38 ganglion cell types in the primate retina for the design of visual prostheses. *The*  
39 *Journal of neuroscience : the official journal of the Society for Neuroscience*  
40 2013;33:7194-7205.
- 41 34. Lorach H, Goetz G, Mandel Y, et al. Performance of photovoltaic arrays in-vivo  
42 and characteristics of prosthetic vision in animals with retinal degeneration.  
43 *Vision Res* 2014.
- 44 35. Shapley RM, Enroth-Cugell C. Visual Adaptation and Retinal Gain Controls. In:  
45 Osborne N, Chader G (eds), *Progress in Retinal Research*. Oxford; 1984:263-  
46 346.

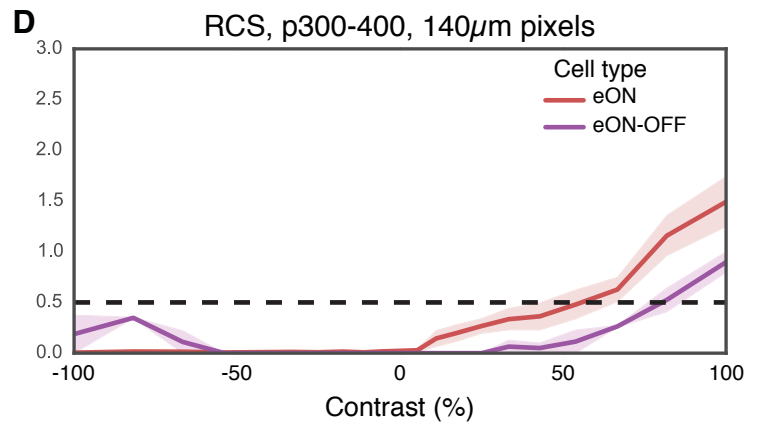
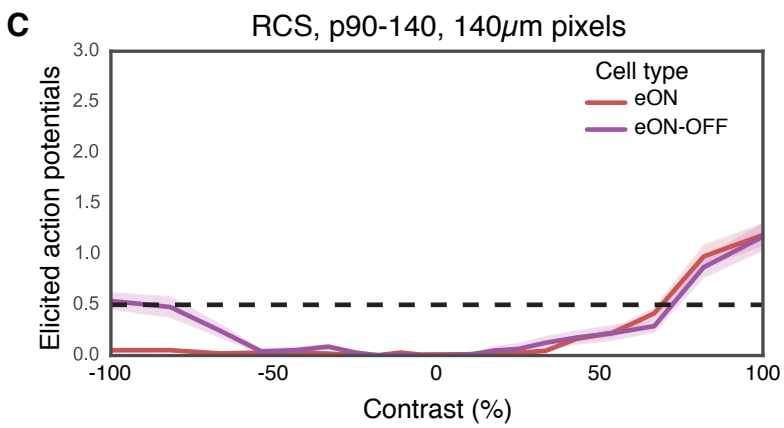
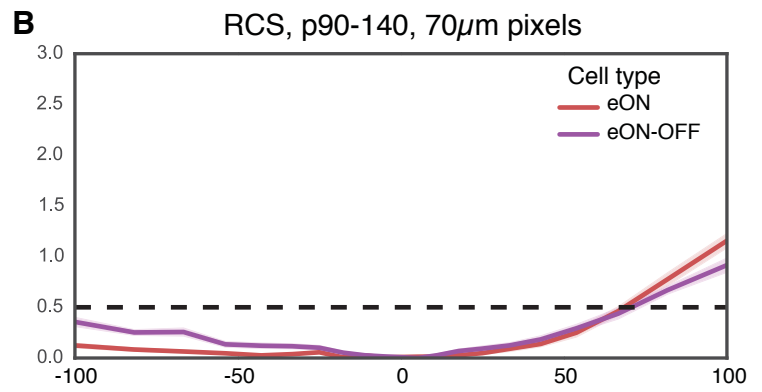
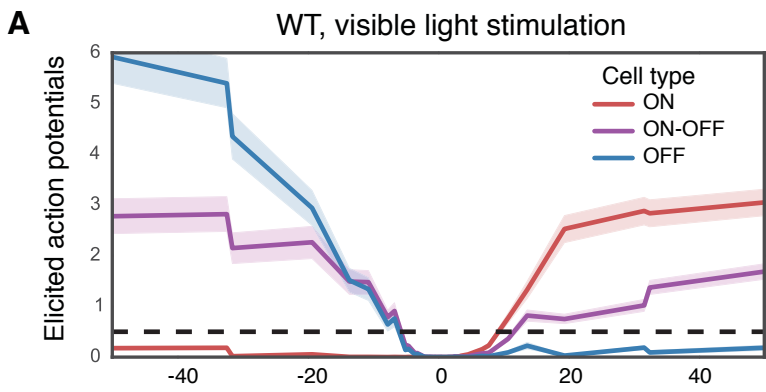
- 1 36. Shapley RM, Kaplan E, Purpura KP. Contrast Sensitivity and Light Adaptation in  
2 Photoreceptors or in the Retinal Network. In: Shapley RM, Lam DM-K (eds),  
3 *Contrast sensitivity*: M.I.T. Press; 1993:103-116.
- 4 37. Shapley RM. Retinal physiology: Adapting to the changing scene. *Current*  
5 *Biology* 1997;7:R412-R423.
- 6 38. McCamy MB, Otero-Millan J, Macknik SL, et al. Microsaccadic efficacy and  
7 contribution to foveal and peripheral vision. *The Journal of neuroscience : the*  
8 *official journal of the Society for Neuroscience* 2012;32:9194-9204.
- 9 39. Martinez-Conde S, Macknik SL, Troncoso XG, Hubel DH. Microsaccades: a  
10 neurophysiological analysis. *Trends in Neurosciences* 2009;32:463-475.
- 11 40. Paninski L. Maximum likelihood estimation of cascade point-process neural  
12 encoding models. *Network: Computation in Neural Systems* 2004;15:243-262.
- 13 41. Truccolo W, Eden UT, Fellows MR, Donoghue JP, Brown EN. A point process  
14 framework for relating neural spiking activity to spiking history, neural  
15 ensemble, and extrinsic covariate effects. *Journal of neurophysiology*  
16 2005;93:1074-1089.
- 17 42. Baylor DA, Lamb TD, Yau K-W. The Membrane Current Of Single Rod Outer  
18 Segments. *J Physiol* 1979;288:589-611.
- 19 43. Rieke F, Baylor DA. Single-photon detection by rod cells of the retina. *Reviews*  
20 *of Modern Physics* 1998;70:1027-1036.
- 21 44. van Alphen B, Winkelman BH, Frens MA. Age- and sex-related differences in  
22 contrast sensitivity in C57BL/6 mice. *Invest Ophthalmol Vis Sci* 2009;50:2451-  
23 2458.
- 24 45. Marc RE, Jones BW, Watt CB, Strettoi E. Neural remodeling in retinal  
25 degeneration. *Progress in Retinal and Eye Research* 2003;22:607-655.
- 26 46. Derrington AM, Lennie P. Spatial and Temporal Contrast Sensitivities of  
27 Neurones in Lateral Geniculate Nucleus of Macaque *J Physiol* 1984;357:219-  
28 240.
- 29 47. Kolb H, Mariani A, Gallego A. A second type of horizontal cell in the monkey  
30 retina. *J Comp Neurol* 1980;189:31-44.
- 31 48. Palanker D, Vankov A, Huie P, Baccus S. Design of a high-resolution  
32 optoelectronic retinal prosthesis. *J Neural Eng* 2005;2:S105-120.
- 33 49. Dacey DM. Origins of perception: retinal ganglion cell diversity and the  
34 creation of parallel visual pathways. In: Gazzaniga MS (ed), *The Cognitive*  
35 *Neurosciences*: MIT Press; 2004:281-301.
- 36 50. Hafed ZM, Stingl K, Bartz-Schmidt K U, Gekeler F, Zrenner E. Oculomotor  
37 behavior of blind patients seeing with a subretinal visual implant. *Vision Res*  
38 2015;in press.
- 39 51. Stingl K, Bartz-Schmidt KU, Besch D, et al. Artificial vision with wirelessly  
40 powered subretinal electronic implant alpha-IMS. *Proceedings Biological*  
41 *sciences / The Royal Society* 2013;280:20130077.

42  
43

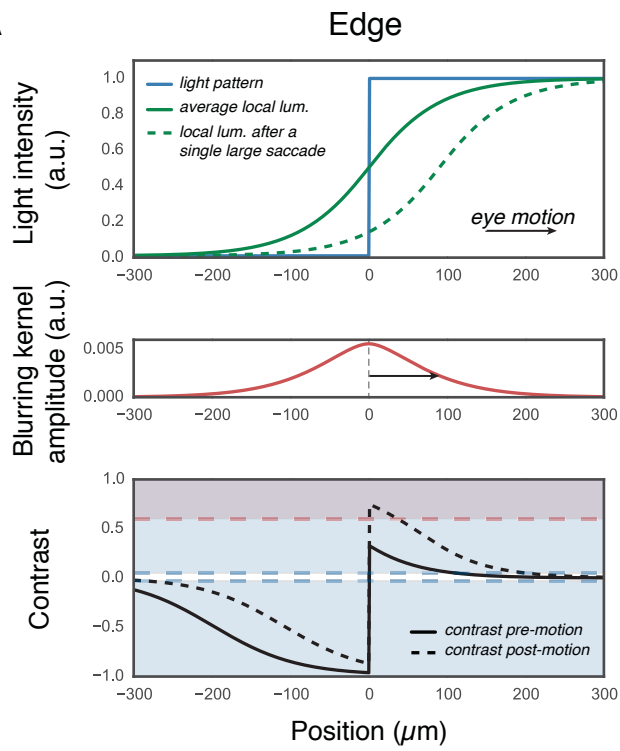










**A****B**